

# Control of etch pit formation for epitaxial growth of graphene on germanium

Cite as: J. Appl. Phys. **126**, 085306 (2019); <https://doi.org/10.1063/1.5108774>

Submitted: 02 May 2019 . Accepted: 05 August 2019 . Published Online: 27 August 2019

Andreas Becker , Christian Wenger , and Jarek Dabrowski 



View Online



Export Citation



CrossMark

Journal of  
Applied Physics

SPECIAL TOPIC:  
Polymer-Grafted Nanoparticles

Submit Today!

AIP  
Publishing

# Control of etch pit formation for epitaxial growth of graphene on germanium

Cite as: J. Appl. Phys. 126, 085306 (2019); doi: 10.1063/1.5108774

Submitted: 2 May 2019 · Accepted: 5 August 2019 ·

Published Online: 27 August 2019



Andreas Becker,<sup>a)</sup> Christian Wenger, and Jarek Dabrowski

## AFFILIATIONS

IHP—Leibniz-Institut für innovative Mikroelektronik, Im Technologiepark 25, 15236 Frankfurt (Oder), Germany

<sup>a)</sup>Author to whom correspondence should be addressed: [becker@ihp-microelectronics.com](mailto:becker@ihp-microelectronics.com)

## ABSTRACT

Graphene epitaxy on germanium by chemical vapor deposition is a promising approach to integrate graphene into microelectronics, but the synthesis is still accompanied by several challenges such as the high process temperature, the reproducibility of growth, and the formation of etch pits during the process. We show that the substrate cleaning by preannealing in molecular hydrogen, which is crucial to successful and reproducible graphene growth, requires a high temperature and dose. During both substrate cleaning and graphene growth, etch pits can develop under certain conditions and disrupt the synthesis process. We explain the mechanisms how these etch pits may form by preferential evaporation of substrate, how substrate topography is related to the state of the cleaning process, and how etch pit formation during graphene growth can be controlled by choice of a sufficiently high precursor flow. Our study explains how graphene can be grown reliably on germanium at high temperature and thereby lays the foundation for further optimization of the growth process.

© 2019 Author(s). All article content, except where otherwise noted, is licensed under a Creative Commons Attribution (CC BY) license (<http://creativecommons.org/licenses/by/4.0/>). <https://doi.org/10.1063/1.5108774>

## I. INTRODUCTION

The unique properties of graphene, such as its flat form factor, its high carrier mobility, its tunable Fermi level, and its plasmonic activity, make this material a candidate for a variety of applications in microelectronics, such as radiofrequency electronics,<sup>1</sup> optoelectronics,<sup>2–4</sup> and chemical sensing.<sup>5</sup>

However, large-scale implementation of graphene in microelectronics is, to date, obstructed by the difficulties of synthesis and integration of the graphene film into mainstream CMOS technology. For example, stringent purity requirements obstruct the use of some well-investigated metallic substrates like copper for integration into front-end-of-line processing, because contaminants stick to the graphene even when the film is delaminated and cleaned.<sup>6,7</sup> Additional process and substrate requirements depend on the details of integration. One investigated approach is delamination of graphene from the substrate and transfer to a target wafer.<sup>8</sup> Challenges of such transfer may be to ensure its reliability, the introduction of defects, that the interface between graphene and target wafer may get contaminated, and that large-scale implementation would require the development of automation. Further integration approaches are the transfer by

bonding of a graphene-covered wafer to the target wafer<sup>9,10</sup> and the direct synthesis on the target wafer.

For all these integration schemes, germanium is a promising substrate because it can be grown epitaxially on silicon, and wafer-scale graphene growth on germanium from a mixture of hydrogen and methane has been demonstrated.<sup>11–13</sup> For approaches involving transfer, Ge(110) is so far more promising than Ge(001) in view of the higher reported quality of graphene grown on Ge(110).<sup>11</sup> For direct integration of the growth process, Ge(001) has the advantage of being compatible to the standard Si(001) wafer orientation. In this work, we focus on Ge(001). To date, accompanying challenges are the poor electrical quality of gr/Ge(001),<sup>12</sup> the faceting of the substrate under gr/Ge(001),<sup>14,15</sup> and the high synthesis temperature. To solve these challenges, a better understanding of the growth process is necessary. For example, substrate cleaning for graphene growth on germanium has not received enough attention in the literature, as reported growth procedures usually just mention a ramp-up of the sample temperature in a hydrogen-filled chamber, before admitting the precursor. Accordingly, in this paper, we present basic aspects of gr/Ge(001) synthesis, focusing on substrate cleaning and how etch pits can form during cleaning and subsequent graphene growth.

## II. EXPERIMENTAL DETAILS

Samples were prepared in a stainless steel UHV chamber with a volume of 6.15 l that can be pumped by a turbomolecular pump or via a bypass by a scroll pump. Hydrogen of purity 99.999% and methane of purity 99.995% can be admitted to the CVD chamber via mass flow controllers. The pressure is regulated by a feedback-controlled downstream leak valve. Samples are heated by a home-built heating stage with a 400 W halogen lamp, and the temperature is feedback-controlled using a pyrometer that has been calibrated to the melting point of bulk germanium. We also tested direct current heating as an alternative heating method and then discarded it, because the temperature was very inhomogeneous. For analysis with surface-science analysis methods, processed samples can be transferred *in situ* to the attached UHV cluster tool, whose chambers have base pressures of about  $10^{-10}$  mbar.

The substrate used in the experiments is  $2\ \mu\text{m}$  thick undoped epitaxial Ge/Si(001) that was stored in air for several months. The samples were loaded as pieces of  $6.5 \times 6.5\ \text{mm}^2$  size. The temperature ramp-up from room temperature to  $930\ \text{C}$  was carried out within 5 min using a linear ramp. Before growing graphene on the samples, they were cleaned by annealing in hydrogen at  $930\ \text{C}$ , using 80 mbar for 15 min or 100 mbar for 30 min. We discuss the origin and importance of these cleaning parameters later. Then, the pressure was reduced to the synthesis pressure of 10 mbar, the hydrogen flow was set to 25 sccm, and the methane precursor was admitted.

Select specimens were characterized by optical microscopy, scanning electron microscopy (SEM), Raman spectroscopy with an excitation wavelength of 532 nm, and *in situ* scanning tunneling microscopy (STM). Differential interference contrast in the reflected light optical microscope enabled investigation of the surface topography evolution.

## III. RESULTS AND DISCUSSION

### A. Cleaning germanium by annealing in hydrogen

#### 1. Importance of substrate cleaning

It is already established in the literature that oxygen contamination on germanium desorbs upon annealing at  $450\text{--}500\ \text{C}$ ,<sup>16</sup> whereas under ultrahigh vacuum conditions, carbon contamination sticks at any temperature below the melting point of germanium.<sup>17</sup> The latter observation is plausible according to our *ab initio* calculations, because the Ge–C binding energy of about 4 eV prevents substantial carbon desorption below the melting point of germanium, and atomic size mismatch results in a low solubility of carbon in bulk germanium. Carbon contamination may be expected to impede graphene growth, because the contaminants would act as seeds. On the other hand, some authors suggested that ripening of adsorbed “carbon precursor phases” to graphene crystals might occur.<sup>18</sup>

To resolve this question, we first used *in situ* STM to investigate surface evolution of an air-contaminated Ge/Si(001) sample during annealing at  $930\ \text{C}$  in 10 mbar pure hydrogen. As we show later, etch pits formed, but the presented STM scans are from regions between the pits. After 15 min annealing, at the large scale, the surface is completely covered with contamination, and typical Ge(001) terraces and steps are not visible, see Fig. 1(a). After 45 min annealing, at the small scale, we observe many small clusters with a

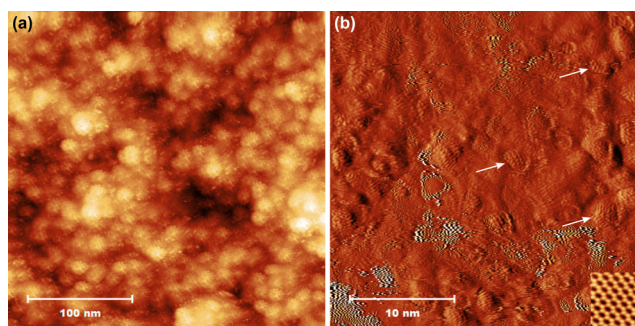
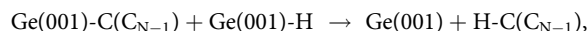


**FIG. 1.** STM images of a Ge/Si(001) surface after annealing at  $930\ \text{C}$  in 10 mbar  $\text{H}_2$  for (a) 15 min and (b) 45 min. The bias voltages were (a)  $-2\ \text{V}$  and (b)  $-50\ \text{mV}$ . Arrows mark examples of regions where the graphene lattice can be recognized. The inset in (b) shows a clean  $c(4 \times 2)$  reconstructed Ge(001) surface at bias voltage  $-1\ \text{V}$  for comparison, at the same scale as in the differentiated parent image.

graphenelike lattice, see Fig. 1(b). Loose adsorbates impede imaging in the areas between these clusters, and features of the clean Ge(001) surface are nowhere to be seen. The presence of graphenelike clusters implies that air-borne carbon contamination, carbon contamination originating from chamber outgassing, or carbon impurities in the gas polymerize on the surface during the annealing. However, despite the long annealing time, the clusters remain very small and defective, which means that they cannot be expected to ripen into macroscopic high-quality graphene flakes. We conclude that without precleaning, carbon contamination on Ge(001) precludes the growth of high-quality graphene.

#### 2. Substrate cleaning using molecular hydrogen

That molecular hydrogen may adsorb dissociatively on germanium is indicated by experimental investigations and the well-described dissociation of molecular hydrogen on silicon,<sup>19,20</sup> which is chemically similar to germanium. Indeed, from our *ab initio* calculations done with the HSE06<sup>21</sup> (PBE<sup>22</sup>) exchange-correlation functionals, we estimate the dissociative adsorption of  $\text{H}_2$  on Ge(001)  $p(2 \times 1)$  to occur with a small energy barrier of 0.5 eV (0.3 eV), corresponding to about 5 kT (3 kT) at  $930\ \text{C}$ , whereas the barrier for associative desorption is substantially higher, amounting to 1.7 eV (1.3 eV). Furthermore, the calculations prove that surface reactions of the type



in which a hydrogen atom detaches from Ge(001) and opens a C–Ge bond of an adsorbed  $\text{C}_N$  cluster to saturate the C atom previously bonded to Ge, are usually favorable energetically and can eventually lead to desorption of the cluster, provided the surface concentration of H is sufficiently high and  $N$  is small enough. Therefore, we can *a priori* expect that annealing germanium in molecular hydrogen causes catalytic hydrogenation of chemisorbed carbon contaminants and their subsequent desorption.

To find suitable cleaning parameters, we annealed Ge/Si(001) substrates at 930 °C for 15 min at different hydrogen pressures, see Fig. 2. As described in Sec. III A 1, 10 mbar is by far not enough for complete cleaning and results in deep pyramidal etch pits and a network of polymerized carbon between the etch pits. But with increasing pressure, the etch pits become flatter and their shape becomes more rounded. With 30 mbar, there are still pyramidal etch pits, but with 50 mbar, the topography is determined by shallow round depressions, which resemble residues of etch pits. With 80 mbar, faint perpendicular ridges are present. These ridges correspond to the well-known cross-hatch pattern that reflects the distribution of strain near the surface.<sup>23</sup> These strain undulations are caused by misfit dislocations in the germanium layer that form to relax the strain induced by the lattice-mismatched Ge/Si(001) interface. Furthermore, we annealed Ge/Si(001) at 40 mbar and 930 °C for 30 min (not shown) and obtained a faint cross-hatch pattern similar to the surface in Fig. 2(d). Compared to Fig. 2(b), the pits have been filled. This indicates that the time-dependent evolution is qualitatively similar to the pressure-dependent evolution of the surface.

We propose that the described etch pits form due to preferential substrate loss near threading dislocations and are kinetically stabilized by contamination-induced inhibition of surface diffusion. Initially, we expect strain-driven formation of only shallow etch pits where threading segments intercept the surface. These initial topographic depressions result in locally increased step density and curvature, which leads to further preferential evaporation by a kinetic mechanism. Germanium adatoms diffusing on a clean surface would refill such pits, but Ge–C bonds are expected to block the diffusion path, impeding the adatom diffusion on a carbon-contaminated surface. The observed flattening of etch pits with increasing hydrogen dose is thus explained by the associated

decrease in the concentration of carbon contamination and, consequently, by increased mobility of the adatoms.

To investigate the effect of temperature on the cleaning, we carried out the hydrogen annealing at 850 °C, 80 mbar for 15 min. The resulting surface featured deep pyramidal etch pits (not shown), which indicates only incomplete cleaning. This confirms the expectation that carbon removal is slower at lower temperature. One may counterbalance this to a certain extent by increasing the hydrogen pressure. But since our setup is supplied with a limited amount of gas, we opt to run the cleaning at 930 °C, although a lower process temperature would be strongly desirable for technological integration.

In the light of these facts, one should reinterpret the observations reported by Persichetti *et al.*,<sup>24</sup> who investigated etch pits that formed on germanium during annealing cycles in UHV. The lack of knowledge that the etch pits form only when the surface is covered with carbon has led to some misinterpretations, as discussed in the following.

First, deep etch pits cannot form due to material being “transferred from high-strain regions to more relaxed areas” by surface diffusion. Besides the elaborated fact that the equilibrium topography is a cross-hatch pattern, one reason is that the sometimes observed depressed area around etch pits and the absence of mounds around etch pits, see Fig. 3(a), support the opposite direction of material transport. Moreover, molecular beam deposition of germanium onto a carbon-contaminated uncleaned Ge(001) substrate leads to the formation of crystallites; cf. Fig. 3(b). Before deposition at 500 °C, the substrate was just degassed at 788 °C, which removes oxide but leaves carbon contamination on the surface. This means that if significant amounts of germanium would flow out of the etch pit, it would not wet the contaminated substrate but lead to particle formation around etch pits, which is not observed. It follows that material loss from etch pits occurs mainly by evaporation.

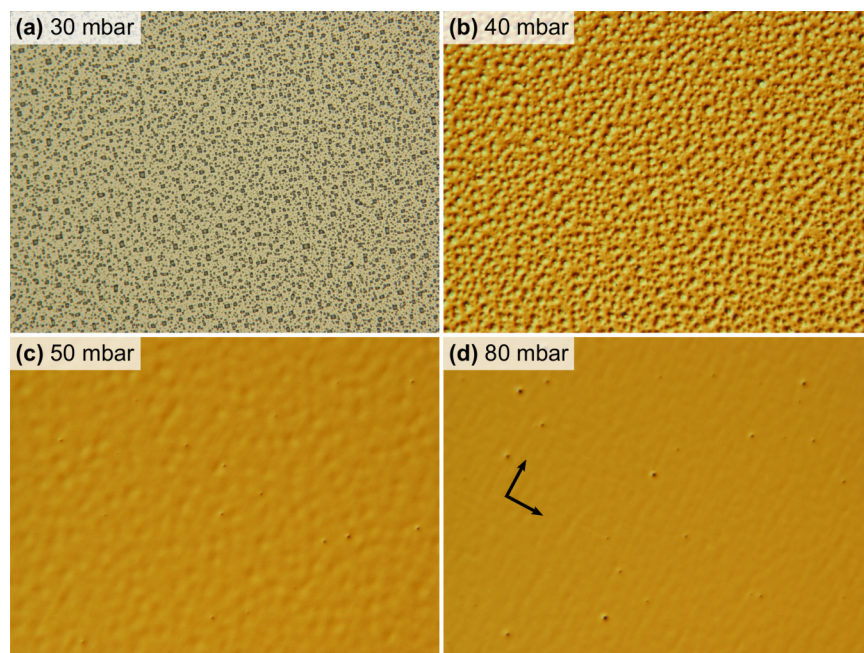


**FIG. 2.** Optical micrographs of the Ge/Si(001) surface after annealing for 15 min at 930 °C in hydrogen with a pressure of (a) 30 mbar, (b) 40 mbar, (c) 50 mbar, and (d) 80 mbar. The width of each shown area is 255  $\mu\text{m}$ . (a) was captured in bright-field mode and (b)–(d) with differential interference contrast, which increases the height contrast. The arrows in (d) mark the directions of the ridges of the evolving cross-hatch pattern.

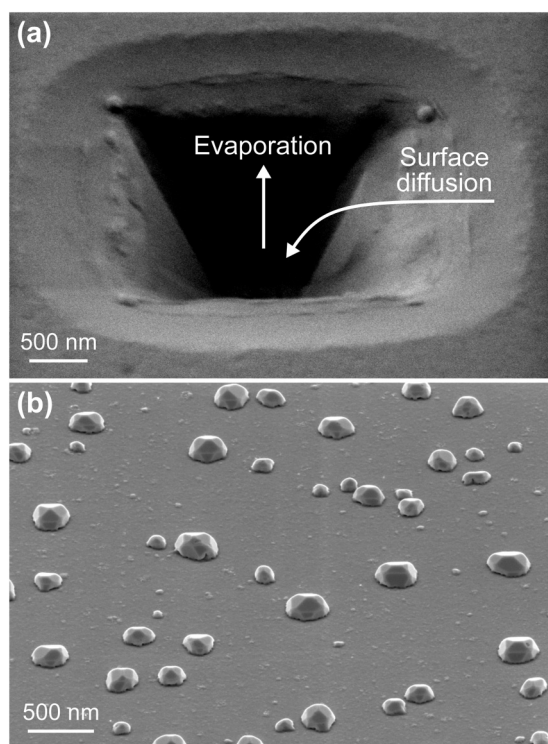


**FIG. 3.** (a) SEM image of an etch pit on Ge(001) with a pyramidal center and a rounded, depressed edge. According to our model, material is removed from the etch pit by substrate evaporation and simultaneously the pit is refilled by surface diffusion of substrate from the edge into the pit. (b) SEM image of crystallites formed by germanium deposition on carbon-contaminated Ge(001) at 500 °C.

Second, in contrast to the assumptions by Persichetti *et al.*<sup>24</sup> on the energetic stabilization and shape of the etch pits, we have experimentally demonstrated the instability of deep etch pits on a clean surface. The inclination of the etch pit facets is determined kinetically by the anisotropy of the etching rate; a detailed geometrical treatment is presented by Heimann.<sup>25</sup>

Third, regarding the analysis of Persichetti *et al.*<sup>24</sup> on the etch pit distribution, we point out that only on bulk Ge(001) some of the etch pits were arranged in lines and etch grooves were present, see Fig. 4, whereas on Ge/Si(001) the pits were randomly distributed, see Fig. 2(a). We suggest that the peculiar etch pit distribution on bulk Ge(001) can be explained by additional dislocations generated at scratches in the surface.<sup>26</sup> Mechanical defects such as scratches may be due to poor polishing of the bulk Ge(001), whereas the Ge/Si(001) surface has not been polished.

## B. Graphene growth on Ge(001)

### 1. Effect of residual contamination

We found that residual contamination left after substrate cleaning by annealing in hydrogen at 930 °C, 80 mbar for 15 min causes the formation of dark spots in SEM images of subsequently

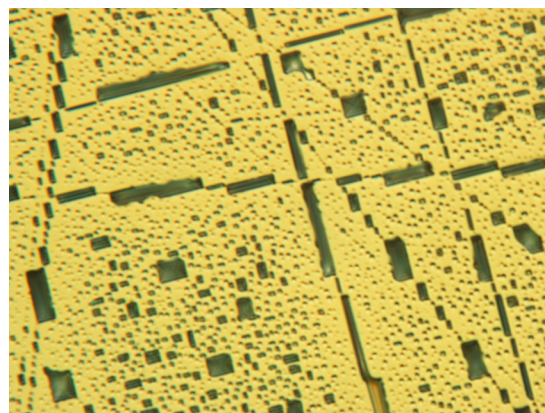


**FIG. 4.** Optical micrograph (57 μm width, differential interference contrast) of a bulk Ge(001) surface after annealing at 900 °C in a mixture of hydrogen and hydrocarbon, showing etch grooves and pyramidal etch pits, some of which are arranged in randomly oriented lines.

grown graphene, like in Fig. 5, which we interpret as graphene multilayers growing under the primary graphene layer. More thorough cleaning by cycles of sputtering and annealing, or by degassing the sample in high vacuum and annealing in 100 mbar hydrogen at 930 °C for 30 min, used for cleaning the sample shown in Fig. 6(a), strongly reduced the density of multilayer islands. However, on all samples we have grown at 930 °C and 10 mbar total pressure, we observed contamination particles such as those visible as the white spots in Fig. 6(a).

Scaparro *et al.*<sup>27</sup> and Pasternak *et al.*<sup>28</sup> observed multilayer nucleation before completion of the first monolayer when using a sufficiently high precursor flow. They argue that it is the high carbon supersaturation that enables the multilayer nucleation. While this might be true, an additional possibility is that a high precursor flow results in a faster rise of the precursor partial pressure and thus in reduced cleaning time, which could promote contamination-induced multilayer formation.

### 2. Control of etch pit formation

We also observed etch pit formation during graphene growth. With 6 sccm methane flow, small depressions were present after 60 min, see Figs. 5(a) and 5(c). After in total 90 min, these depressions have deepened to etch pits, see Fig. 5(b). We are sure that this sample with etch pits is not an outlier, because we observed etch pit formation during graphene growth under a variety of process conditions involving different temperatures (down to 800 °C) and total pressures (5 mbar, 10 mbar, 20 mbar at 930 °C).

Etch pit formation during graphene growth can be explained in the same way as etch pit formation during substrate cleaning: When graphene coverage of the substrate is not complete, substrate evaporates, and it evaporates preferentially near dislocations. When at the same time the graphene coverage is sufficiently high, surface diffusion may be inhibited compared to the clean surface, and hence the inhomogeneous evaporation leads to pits. Such inhibition

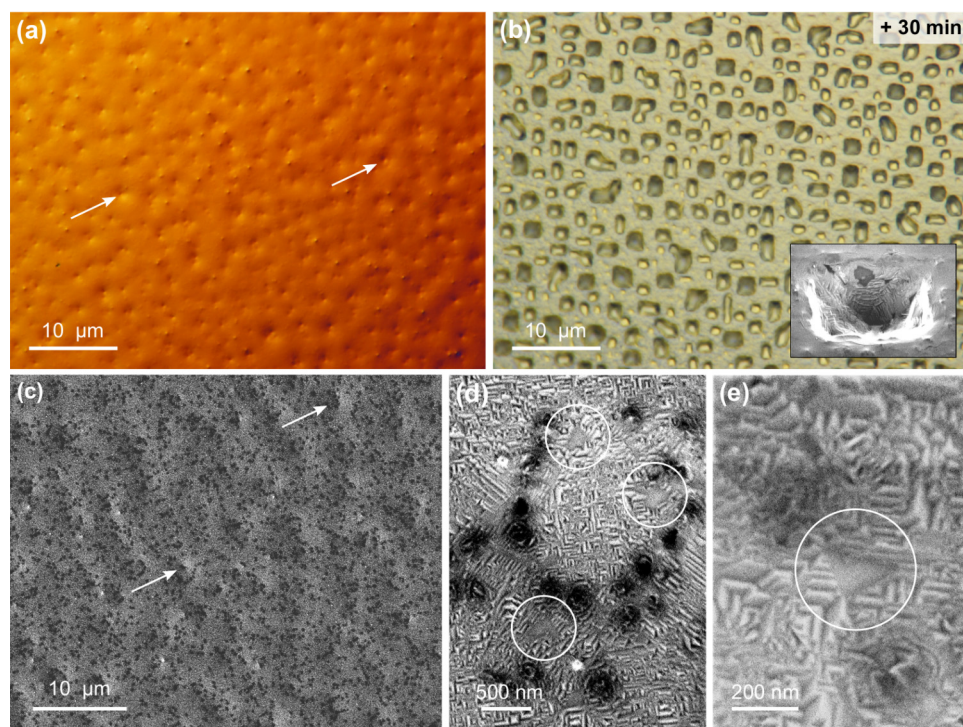


**FIG. 5.** (a) Optical micrograph with differential interference contrast of gr/Ge(001) grown with 6 sccm methane for 60 min after substrate cleaning in 80 mbar hydrogen for 15 min. Arrows mark examples of topographic depressions. (b) Bright-field optical micrograph of a sample grown with 6 sccm for 90 min, showing deep etch pits. Inset: SEM close-up showing faceted substrate inside an etch pit. (c) SEM image of the sample shown in (a), where arrows mark examples of depressions in the topography of the same type as marked in (a). (d) and (e) SEM images zoomed into depressions similar to those marked in (c). Circles mark unfaceted areas, which correspond to holes in the graphene sheet with about 200 nm diameter. The numerous small black spots in (c)–(e) correspond to multilayer graphene flakes. These SEM images were captured with a High Efficiency Secondary Electron Detector (HE-SE2) that increases the topographic contrast.

of surface diffusion is likely to occur due to Ge–C bonds at edges of graphene flakes, whereas a high mobility of substrate atoms under the basal plane of graphene is indicated by facet formation. In line with our model of etch pit formation, inside the depressions on the sample shown in Fig. 5(a) we found small areas of uncovered substrate with a diameter of 200 nm, see Figs. 5(d) and 5(e). These uncovered areas enable evaporation that is necessary for etch pit formation. The persistence of small holes in graphene at 6 sccm and below makes it clear that graphene growth slows down or possibly even stops near completion of the first monolayer.

Etch pits did not form when we used a sufficiently high precursor flow, for example, 7 sccm, see Fig. 6. To correctly interpret Fig. 6(a), we point out the inhomogeneous dissolution of the facets when the graphene coverage becomes complete. This is why facets can only be recognized in some places in this image. To compare, after 35 min growth at 7 sccm (not shown), we observed more pronounced faceting and still small uncovered substrate areas. This is why we are sure that after 40 min at 7 sccm, the surface was completely covered with graphene. After prolonged growth at 60 min, neither topographic depressions like in Fig. 5(a) nor etch pits were obtained. Apparently, 7 sccm precursor flow enables complete closure of the graphene layer before etch pits can form.

The 2D band in the Raman spectrum of this sample, shown in the inset of Fig. 6(a), corroborates the presence of graphene and the intense D band with a D/G intensity ratio of 60% indicates a fairly high density of defects. The defect density is probably mainly determined by grain boundaries arising due to the fourfold symmetry of the substrate. The high defect density would hence be caused by a small grain size due to the fast growth. In future work, it

would be possible to reduce the defect density by beginning the process with slow growth and only near completion of full coverage switching to a higher flow to avoid etch pit formation. The reason why literature reports higher quality of gr/Ge(001) without etch pits despite using a fixed precursor flow<sup>12,27,29</sup> may lie in the volume in the process chamber: A larger chamber naturally leads to a more gradual rise of the precursor partial pressure.

Formation of suspended graphene over Ge(110) and Ge(111) substrate cavities, which we interpret as etch pits, has been observed during growth of nanocrystalline graphene on germanium through graphitization of a polymer layer by Yekani *et al.*<sup>30</sup> We suppose that the cavities could form under the polymer layer because the graphitizing polymer may have been permeable to evaporating substrate and had sufficiently low adhesion to the substrate. In contrast, the etch pits we obtained during graphene growth on Ge(001) were not covered by suspended graphene, see the inset in Fig. 5(b). Faceting of the substrate inside etch pits indicates that our graphene rather kept sticking to the substrate while the pits formed. This difference in sticking behavior may be due to differences in the substrate orientations or in the graphene growth methods.

When adapting our parameters to a different setup, it should be taken into account the inevitable uncertainty in the temperature calibration and the fact that our reactor walls and our gas phase are cold. Concerning the effect of gas-phase temperature, methane may undergo pyrolysis and form higher-order hydrocarbons,<sup>31–35</sup> which might have lower adsorption barriers on the substrate than methane. For example, according to our calculations, the barrier for dissociative adsorption of C<sub>2</sub>H<sub>4</sub> is lower (0.8 eV) than that for

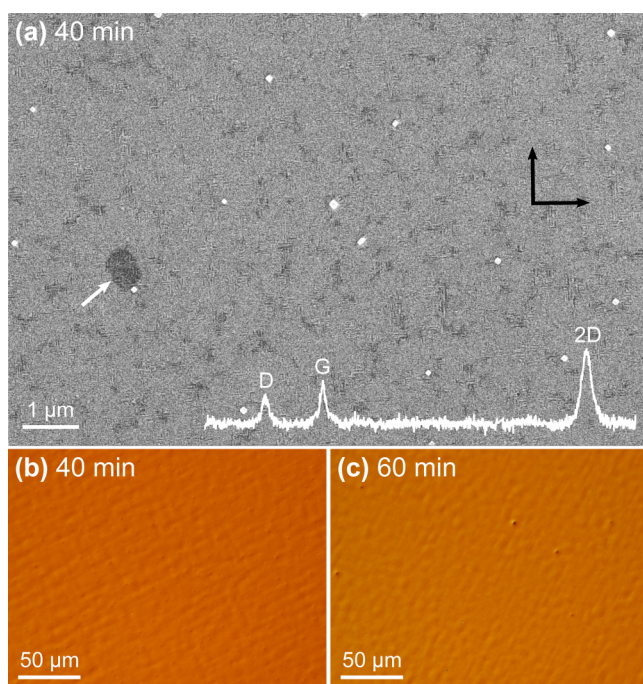


**FIG. 6.** (a) SEM image of a graphene layer on Ge(001), grown with 7 sccm methane for 40 min after substrate cleaning by annealing in 100 mbar hydrogen for 30 min. The white arrow marks one of the very few remaining contamination-induced multilayers. Black arrows mark the  $\langle 100 \rangle$  directions parallel to the facet ridges. Contrast variations are due to the substrate facets being in different states of dissolution among the sample. The inset shows a Raman spectrum of the sample at wavenumbers from  $1100$  to  $2900 \text{ cm}^{-1}$ . Peaks due to oxygen and nitrogen in air have been removed. (b) and (c) Optical micrographs with differential interference contrast of gr/Ge(001) grown with 7 sccm methane for 40 min and 60 min, respectively, demonstrating surfaces without etch pits, but instead with cross-hatch patterns.

$\text{CH}_4$  (1.2 eV) on Ge(001). In addition, how quickly the precursor growth parallel pressure in the chamber increases after admitting depends on the volume of the chamber.

#### IV. CONCLUSIONS

Removal of carbon contamination from germanium is necessary for graphene growth and can be achieved by annealing in molecular hydrogen. Optical microscopy is a simple method to indirectly investigate and optimize this process. Indicators of a successful cleaning process are the absence of etch pits and particles and emergence of a cross-hatch pattern. Usually the reported growth procedures in the literature consist of filling the chamber with hydrogen, ramping up the temperature to the growth temperature, and then admitting the precursor. During this ramp-up of the temperature, the cleaning must occur. To optimize the entire process, we suggest optimizing the cleaning and the growth step separately; for example, different temperatures and total pressures can be used for each step.

Graphene growth by annealing the cleaned Ge(001) surface in a mixture of hydrocarbon precursor and hydrogen can be impaired

by the formation of etch pits that form due to inhomogeneous substrate evaporation before the graphene sheet is closed. Such etch pit formation can be avoided by using a sufficiently high precursor flow. Because a high precursor flow may result in a high nucleation density and thus low graphene quality, we suggest ramping up the precursor flow during the process to achieve a high-quality closed layer.

#### ACKNOWLEDGMENTS

The authors gratefully acknowledge the Gauss Centre for Supercomputing e.V. ([www.gauss-centre.eu](http://www.gauss-centre.eu)) for funding this project by providing computing time through the John von Neumann Institute for Computing (NIC) on the GCS Supercomputer JUWELS at Jülich Supercomputing Centre (JSC) for Project No. hfo06.

#### REFERENCES

- Liao and X. Duan, "Graphene for radio frequency electronics," *Mater. Today* **15**, 328–338 (2012).
- F. Bonaccorso, Z. Sun, T. Hasan, and A. C. Ferrari, "Graphene photonics and optoelectronics," *Nat. Photonics* **4**, 611–622 (2010).
- M. Liu, X. Yin, E. Ulin-Avila, B. Geng, T. Zentgraf, L. Ju, F. Wang, and X. Zhang, "A graphene-based broadband optical modulator," *Nature* **474**, 64–67 (2011).
- Z. Sun, A. Martinez, and F. Wang, "Optical modulators with 2D layered materials," *Nat. Photonics* **10**, 227–238 (2016).
- T. Low and P. Avouris, "Graphene plasmonics for terahertz to mid-infrared applications," *ACS Nano* **8**, 1086–1101 (2014).
- A. Ambrosi and M. Pumera, "The CVD graphene transfer procedure introduces metallic impurities which alter the graphene electrochemical properties," *Nanoscale* **6**, 472–476 (2014).
- G. Lupina, J. Kitzmann, I. Costina, M. Lukosius, C. Wenger, A. Wolff, S. Vaziri, M. Östling, I. Pasternak, A. Krajewska *et al.*, "Residual metallic contamination of transferred chemical vapor deposited graphene," *ACS Nano* **9**, 4776–4785 (2015).
- J. W. Suk, A. Kitt, C. W. Magnuson, Y. Hao, S. Ahmed, J. An, A. K. Swan, B. B. Goldberg, and R. S. Ruoff, "Transfer of CVD-grown monolayer graphene onto arbitrary substrates," *ACS Nano* **5**, 6916–6924 (2011).
- M. Inac, G. Lupina, M. Wietstruck, M. Lisker, M. Fraschke, A. Mai, F. Coccetti, and M. Kaynak, "200 mm wafer level graphene transfer by wafer bonding technique," in *2017 47th European Solid-State Device Research Conference (ESSDERC)* (IEEE, 2017).
- R. Dong, Z. Guo, J. Palmer, Y. Hu, M. Ruan, J. Hankinson, J. Kunc, S. K. Bhattacharya, C. Berger, and W. A. de Heer, "Wafer bonding solution to epitaxial graphene-silicon integration," *J. Phys. D Appl. Phys.* **47**, 094001 (2014).
- J.-H. Lee, E. K. Lee, W.-J. Joo, Y. Jang, B.-S. Kim, J. Y. Lim, S.-H. Choi, S. J. Ahn, J. R. Ahn, M.-H. Park *et al.*, "Wafer-scale growth of single-crystal monolayer graphene on reusable hydrogen-terminated germanium," *Science* **344**, 286–289 (2014).
- M. Lukosius, J. Dabrowski, J. Kitzmann, O. Fursenko, F. Akhtar, M. Lisker, G. Lippert, S. Schulze, Y. Yamamoto, M. A. Schubert *et al.*, "Metal-free CVD graphene synthesis on 200 mm Ge/Si(001) substrates," *ACS Appl. Mater. Interfaces* **8**, 33786–33793 (2016).
- I. Pasternak, P. Dabrowski, P. Ciepielewski, V. Kolkovsky, Z. Klusek, J. M. Baranowski, and W. Strupinski, "Large-area high-quality graphene on Ge(001)/Si(001) substrates," *Nanoscale* **8**, 11241–11247 (2016).
- R. M. Jacobberger, B. Kiraly, M. Fortin-Deschenes, P. L. Levesque, K. M. McElhinny, G. J. Brady, R. R. Delgado, S. S. Roy, A. Mannix, M. G. Lagally *et al.*, "Direct oriented growth of armchair graphene nanoribbons on germanium," *Nat. Commun.* **6**, 8006 (2015).

- <sup>15</sup>K. M. McElhinny, R. M. Jacobberger, A. J. Zaugg, M. S. Arnold, and P. G. Evans, "Graphene-induced Ge(001) surface faceting," *Surf. Sci.* **647**, 90–95 (2016).
- <sup>16</sup>J. Oh and J. C. Campbell, "Thermal desorption of Ge native oxides and loss of Ge from the surface," *Mater. Sci. Semicond. Process.* **13**, 185–188 (2010).
- <sup>17</sup>S. Gan, L. Li, T. Nguyen, H. Qi, R. F. Hicks, and M. Yang, "Scanning tunneling microscopy of chemically cleaned germanium (100) surfaces," *Surf. Sci.* **395**, 69–74 (1998).
- <sup>18</sup>L. Di Gaspare, A. M. Scaparro, M. Fanfoni, L. Fazi, A. Sgarlata, A. Notargiacomo, V. Miseikis, C. Coletti, and M. D. Seta, "Early stage of CVD graphene synthesis on Ge(001) substrate," *Carbon* **134**, 183–188 (2018).
- <sup>19</sup>A. Saedi, B. Poelsema, and H. J. W. Zandvliet, "Hydrogen adsorption configurations on Ge(001) probed with STM," *Phys. Rev. B* **79**, 153402 (2009).
- <sup>20</sup>M. Dürr and U. Höfer, "Dissociative adsorption of molecular hydrogen on silicon surfaces," *Surf. Sci. Rep.* **61**, 465–526 (2006).
- <sup>21</sup>J. Heyd, G. E. Scuseria, and M. Ernzerhof, "Hybrid functionals based on a screened Coulomb potential," *J. Chem. Phys.* **118**, 8207–8215 (2003).
- <sup>22</sup>J. P. Perdew, K. Burke, and M. Ernzerhof, "Generalized gradient approximation made simple," *Phys. Rev. Lett.* **77**, 3865–3868 (1996).
- <sup>23</sup>H. Chen, Y. K. Li, C. S. Peng, H. F. Liu, Y. L. Liu, Q. Huang, J. M. Zhou, and Q.-K. Xue, "Crosshatching on a SiGe film grown on a Si(001) substrate studied by Raman mapping and atomic force microscopy," *Phys. Rev. B* **65**, 233303 (2002).
- <sup>24</sup>L. Persichetti, M. Fanfoni, M. D. Seta, L. De Gaspare, L. Ottaviano, C. Goletti, and A. Sgarlata, "Formation of extended thermal etch pits on annealed Ge wafers," *Appl. Surf. Sci.* **462**, 86–94 (2018).
- <sup>25</sup>R. B. Heimann, *Auflösung von Kristallen* (Springer, Vienna, 1975).
- <sup>26</sup>T. Iizuka, Y. Okada, and M. Kikuchi, "Generation of scratch-induced dislocations in silicon and its orientation dependence," *Jpn. J. Appl. Phys.* **4**, 237–238 (1965).
- <sup>27</sup>A. M. Scaparro, V. Miseikis, C. Coletti, A. Notargiacomo, M. Pea, M. De Seta, and L. D. Gaspare, "Investigating the CVD synthesis of graphene on Ge(100): Toward layer-by-layer growth," *ACS Appl. Mater. Interfaces* **8**, 33083–33090 (2016).
- <sup>28</sup>I. Pasternak, M. Wesolowski, I. Jozwik, M. Lukosius, G. Lupina, P. Dabrowski, J. M. Baranowski, and W. Strupinski, "Graphene growth on Ge(100)/Si(100) substrates by CVD method," *Sci. Rep.* **6**, 21773 (2016).
- <sup>29</sup>C. D. Mendoza, P. G. Caldas, F. L. Freire, and M. E. H. Maia da Costa, "Growth of single-layer graphene on Ge(100) by chemical vapor deposition," *Appl. Surf. Sci.* **447**, 816–821 (2018).
- <sup>30</sup>R. Yekani, E. Rusak, A. Riaz, A. Felten, B. Breitung, S. Dehm, D. Perera, J. Rohrer, C. Rockstuhl, and R. Krupke, "Formation of nanocrystalline graphene on germanium," *Nanoscale* **10**, 12156–12162 (2018).
- <sup>31</sup>Z. J. Hu and K. J. Hüttinger, "Influence of the surface area/volume ratio on the chemistry of carbon deposition from methane," *Carbon* **41**, 1501–1508 (2003).
- <sup>32</sup>C. Guéret, M. Daroux, and F. Billaud, "Methane pyrolysis thermodynamics," *Chem. Eng. Sci.* **52**, 815–827 (1997).
- <sup>33</sup>O. Olsvik, O. A. Rokstad, and A. Holmen, "Pyrolysis of methane in the presence of hydrogen," *Chem. Eng. Technol.* **18**, 349–358 (1995).
- <sup>34</sup>K. Norinaga, O. Deutschmann, and K. J. Hüttinger, "Analysis of gas phase compounds in chemical vapor deposition of carbon from light hydrocarbons," *Carbon* **44**, 1790–1800 (2006).
- <sup>35</sup>M. Somekh, E. Shawat, and G. D. Nessim, "Fully reproducible, low-temperature synthesis of high-quality, few-layer graphene on nickel via preheating of gas precursors using atmospheric pressure chemical vapor deposition," *J. Mater. Chem. A* **2**, 19750–19758 (2014).